Supporting Information

Designing an enzyme assembly line for green cascade processes using bio-orthogonal chemistry

Li Qiao, [#a] Zhiyuan Luo, [#a] Ru Wang, [#b] Xiaolin Pei,[a] Shujiao Wu,[b] Haomin Chen,[a] Tian Xie,*[b] Roger A Sheldon *[c, d] and Anming Wang*[a]

a Key Laboratory of Organosilicon Chemistry and Material Technology, College of Materials, Chemistry and Chemical Engineering. Hangzhou Normal University.No. 2318, Road Yuhangtang, Hangzhou.
E-mail: waming@hznu.edu.cn

b Key Laboratory of Elemene Class Anti-Cancer Medicines, Engineering Laboratory of Development of Chinese Medicines, and Collaborative Innovation Center of Chinese Medicines of Zhejiang Province, Hangzhou Normal University, Hangzhou, Zhejiang, 311121, China; College of Pharmacy, Hangzhou Normal University, Hangzhou, Zhejiang, 311121, China;
E-mail: xbs@hznu.edu.cn

c Molecular Sciences Institute, School of Chemistry, University of the Witwatersrand.PO Wits. 2050, Johannesburg, South Africa.

d Department of Biotechnology, Section BOC, Delft University of Technology. Van der Maasweg 9, 2629 HZ Delft, the Netherlands.
E-mail: r.a.sheldon@tudelft.nl

Table of Contents

Experimental Procedures

1. Materials and Methods

1.1 Materials

The strains *Escherichia coli* DH5α used in the study were ordered from Stratagene, *E. coli C321.ΔA.* and plasmids (pZE21-GFPaav and pEVOL-*p*AzF) obtained from Addgene. The AKR and ADH genes and site-directed mutagenesis primers used in this study were all synthesized by Shanghai Generay Biotech Co. Ltd. The endonuclease and protein markers used were purchased from Takara Products of Hangzhou Haofeng Biotechnology Co., Ltd. The target gene was mutated by whole plasmid site-directed PCR. The plasmid construction and target gene mutation results were sent to Youkang Biotechnology Co., Ltd. Antibiotics (chloramphenicol, kanamycin, and ampicillin) were purchased from Sangon Biotech. (Shanghai). The ncAAs, *p*-AzF and *p*-PaF, were obtained from Artis Biotech Co. Ltd. Anhydrotetracycline hydrochloride (aTc) and dihydro-4,4-dimethyl-2,3-furandione (ketopantolactone) were obtained from Sigma-Aldrich. L-Arabinose and β-nicotinamide adenine dinucleotide phosphate disodium salt were purchased from Sangon Biotech. All other chemical reagents were purchased from Sinopharm Chemical Reagent Ltd. (Shanghai).

E. coli C321.ΔA. was based on EcNR2 [1] (*Escherichia coli* MG1655 *ΔmutS::cat* Δ(*ybhB-bioAB*)::[*λcI857* Δ(*cro-ea59*)::*tetR-bla*]) and has been engineered by Marc J. Lajoie [2]. *E. coli C321.ΔA.* [strain 48998 (www.addgene.org/48998)] is available from addgene.

1.2 Plasmid construction, protein expression and characterization

1.2.1 Plasmid construction

AKR gene (akr, Gene ID: 897867), ADH gene (adh, Gene ID: 4413616) were synthesized at Shanghai Generay Biotech Engineering Co., Ltd. Then, at restriction sites KpnI and Hind III, target genes were ligated into pZE21 from Addgene [3] to acquire pZE21-*akr* and pZE21-*adh* as in our previous report [4]. The constructed recombinant plasmid was transformed into host *E. coli* DH5α after codon optimisation. In principle, each mutation site should keep away from the catalytic triad and active sites in geometric distance to the catalytic pocket. Additionally, Tyr is preferentially selected for mutation for stabilising the enzyme structure as much as possible when ncAAs with similar structure are inserted into the polypeptide chain of the protein. The active sites of AKR include Glu227, Asn276, Lys274, Ser275, and Arg280.[5] To avoid unwanted covalent linkages that can destroy the active site structure, we selected 49(Y), 138(Q), 215(E), and 266(E) mutation sites based on the structure analysis (**Figure S1**, red). Site-directed mutagenesis PCR was carried out to introduce an amber codon (UAG) in place of a tyrosine codon at the selected site. However, the catalytic mechanism of ADH for NADPH regeneration is still unclear using alcohols.[6] We inferred three key binding sites including Lys159, Ser142 and Asn113 based on previous reports of ADH-catalysed dehydrogenation with benzyl alcohol as substrate.[7-9] Thus, in the case of ADH (**Figure S1, blue**), sites such as 155(Y), 189(Y), 3(R), and 251(Q) were preselected and mutated, respectively. According to the selected mutation site, multiple whole plasmid site-directed mutagenesis was performed.

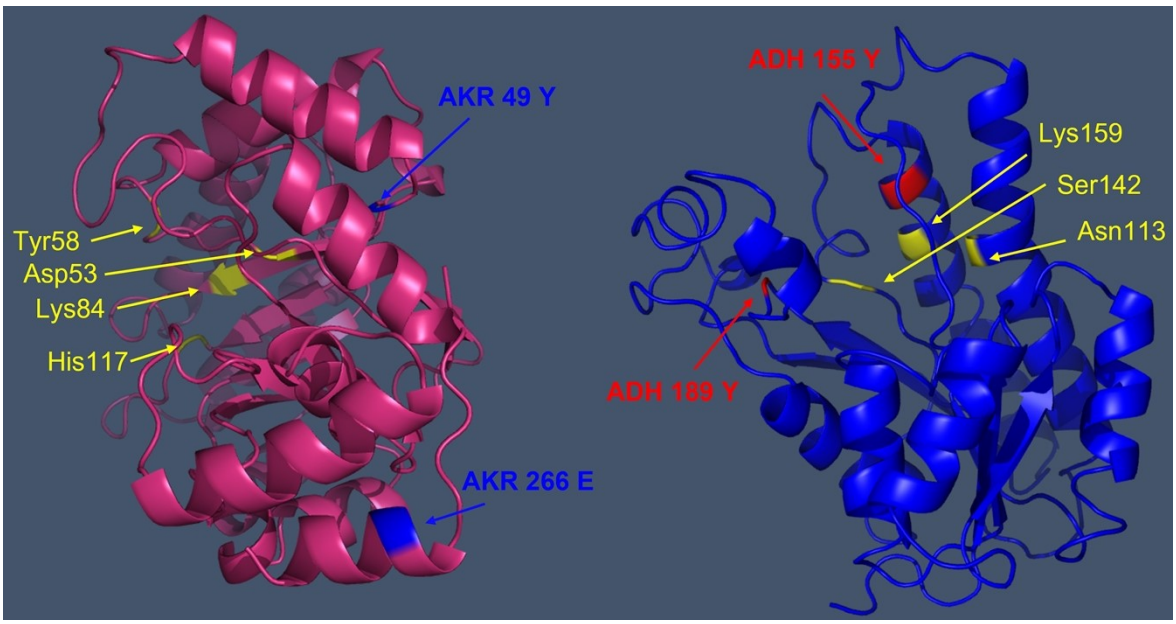

Figure S1. Three-dimensional structure and key amino acids in possible active sites (yellow) for AKR (red) and ADH (blue)

Primers

(1) Site-directed mutagenesis of AKR and ADH

Table S1. Primers for AKR sites mutants

Primers	Sequence (5'→3')	Tm (°C)
akr-49Y-pZE21-F	GCAATTAAAATGGGCTAGACCCATATTGATACC	58
akr-49Y-pZE21-R	GGTATCAATATGGGTCTAGCCCATTTTAATTGC	56
akr-138Q-pZE21-F	GCAGAAGGCGTGCGTTAGGGCTTAATTCGCTAT	66
akr-138Q-pZE21-R	ATAGCGAATTAAGCCCTAACGCACGCCTTCTGC	66
akr-215E-pZE21-F	ACCAAACGCACCTTATAGGAAATTGCCAAAAAT	56
akr-215E-pZE21-R	ATTTTTGGCAATTTCCTATAAGGTGCGTTTGGT	57
akr-266E-pZE21-F	AAACTGAGCGAAGAATAGATGAAACTGCTGGAT	60
akr-266E-pZE21-R	ATCCAGCAGTTTCATCTATTCTTCGCTCAGTTT	62

Table S2. Primers for ADH sites mutants

Primers	Sequence (5'→3')	Tm (°C)
adh-3Y-pZE21-F	TACCGCATGAGCAATTAGCTGGATGGTAAAGTT	56
adh-3Y-pZE21-R	AACTTTACCATCCAGCTAATTGCTCATGCGGTA	54
adh-155Y-pZE21-F	CCGAGCTTAGGTGCCTAGAATGCAAGTAAAGGC	64
adh-155Y-pZE21-R	GCCTTTACTTGCATTCTAGGCACCTAAGCTCGG	61
adh-189Y-pZE21-F	ACCGTTCATCCGGGCTAGATTAAAACCCCGCTG	67
adh-189Y-pZE21-R	CAGCGGGGTTTTAATCTAGCCCGGATGAACGGT	64

adh-251E-pZE21-F	GGCGGCTATACCGCATAGCACCACCACCACCAC	60
adh-251E-pZE21-R	GTGGTGGTGGTGGTGCTATGCGGTATAGCCGCC	62

(2) Replacement of his-tag on ADH with tetracysteine tag

After site directed mutagenesis, his-tag at C-terminal of ADH was replaced by tetracysteine tag (Cys-Cys-Pro-Gly-Cys-Cys) via PCR technic. The primers required for PCR are shown in **Table S3**.

Table S3. Primers for tag exchange

Primers	Sequence (5'→3')	Tm (°C)
Cys-F	CGGGGTACCATGAGCAATCGTCTGGATGG	62
Cys-R	CCCAAGCTTTTAACAACAACCCGGACAACACTGTGCGGTATAGCCGCC	61

1.2.2 Protein expression

The recombinant plasmids, pZE21 harbouring the AKR mutant gene and pEVOL-p-AzF, were co-transformed into *E. coli C321.ΔA.* cells for *p*-Azido-L-phenylalanine (*p*-AzF) incorporation and enzyme proteins expression of mutants including AKR^{49}_{266} (Site 49 and site 266 were mutated) and AKR^{138}_{215} (Site 138 and site 215 were mutated). The recombinant plasmids pZE21-ADH mutant gene and pEVOL-pYlRs were co-transformed into *E. coli C321.ΔA.* cells for *p*-propargyloxy-L-phenylalanine (*p*-PaF) incorporation and enzyme proteins expression of mutants including ADH^{155}_{189} and ADH_{251}.

The strains containing recombinant plasmids were cultured in LB medium with 50 μg·mL^{-1} ampicillin, 34 μg·mL^{-1} chloramphenicol and 100 μg·mL^{-1} kanamycin at 34 °C in a shaking incubator (220 rpm). When the OD_{600} reached 0.6-0.8, the inducer 0.2% (w·v^{-1}) L-arabinose was added. One hour later, another inducer, 30 mg·mL^{-1} aTc, and 1 mmol·mL^{-1} *p*-AzF (*p*-PaF) were added and cultured at 23 °C in a shaking incubator (200 rpm) for 16 h.

1.2.3 Protein characterisation

SDS-PAGE was used to examine the expression of the target enzymes. and matrix-assisted laser desorption ionisation time-of-flight mass spectrometry (MALDI-TOF MS; Bruker Ultraflextreme) was used to further verify their exact relative molecular weight. The sample contained target enzyme-polyhistidine tag, which was purified by immobilised metal ion affinity chromatography with Ni-NTA agarose. And the purified protein solution was collected and concentrated by ultrafiltration tube. Experimental details about characterisation of MALDI-TOF MS are detailed in the supporting information.

1.3 Preparation and characterisation of cross-linked enzymes from cell lysate

1.3.1 Preparation of cross-linked enzymes from cell lysate

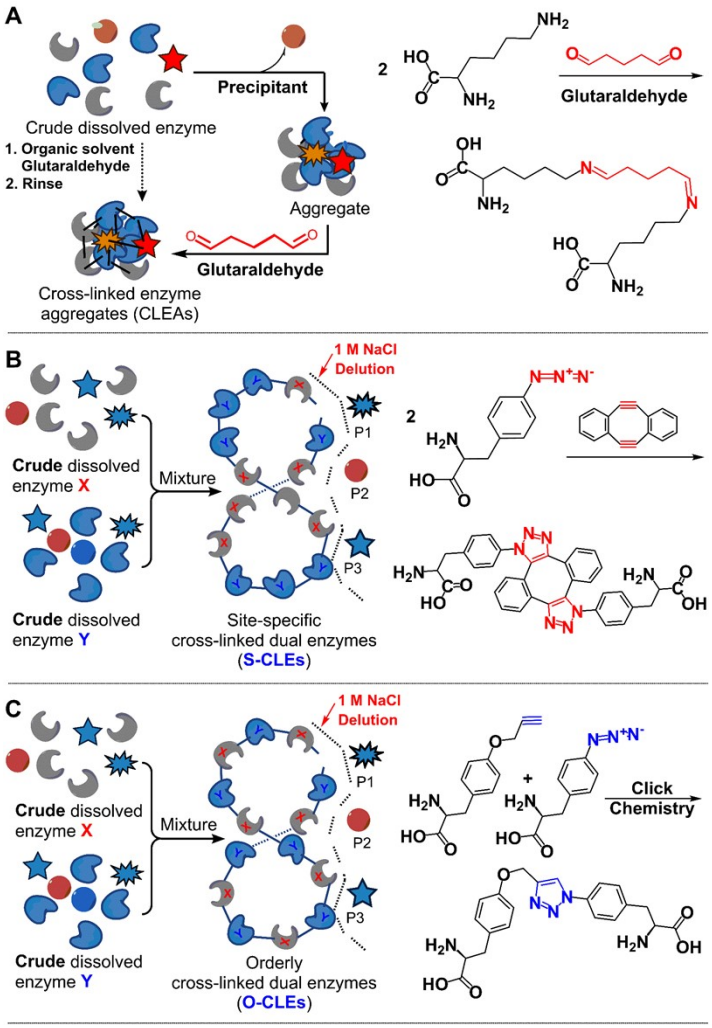

Figure S2. Schematic illustration of combi cross-linked enzymes of AKR and ADH using different methods (A, CLEAs using glutaraldehyde; B, S-CLEs using cyclooctyne; C, O-CLEs using no added crosslinking agents)

The preparation of crosslinked enzyme aggregates (CLEAs, **Figure S2A**) was using glutaraldehyde as crosslinker. Both of the enzymes were purified by Ni-NTA agarose, precipitated using saturated ammonium sulfate solution and then crosslinked with 1.2 wt% glutaraldehyde [10]. Bradford analysis was used to determine the amount of protein remaining in the supernatant.

Preparation system of site-specific cross-linked enzymes (S-CLEs, **Figure S2B**): crude enzyme solution containing *p*-AzF modified AKR mutant (AKR_{266}^{49} or AKR_{215}^{138}), crude enzyme solution containing *p*-AzF modified ADH mutant (ADH_{189}^{155} and ADH_{251}^{3}), dibenzocycloocta-4a,6a-diene-5,11-diyne DBA solution (8 mM). The molecular ratio of the two enzymes was 1:1, and the molecular ratio of acetylene groups in *p*-AzF and crosslinking agent was 1:2.

Cross-linking of the two enzymes in an ordered -X-Y-X-Y- configuration allows for faster transfer of substrate between the two enzymes in a cascade reaction because of close spatial proximity. In order to immobilise enzyme X and enzyme Y in '-X-Y-X-Y-'manner, two *p*-azido-L-phenylalanine and two *p*-propargyloxy-L-phenylalanine residues were inserted in X and Y, respectively. Thus, subsequent cross-coupling in the presence of the copper catalyst, can only occur in the -X-Y-X-Y- sequence. According to the design, the preparation system of ordered crosslinked enzymes (O-CLEs, **Figure S2C**) included crude enzyme solution containing *p*-AzF modified AKR mutants, AKR_{266}^{49} and AKR_{215}^{138}, crude enzyme solution containing *p*-PAF modified ADH mutant (ADH_{189}^{155} and ADH_{251}^{3}), and 0.4 equivalent CuI. The proportion of the two enzymes in the cross-linking reaction was 1:1.

Bio-orthogonal cross-linking reaction was carried out under consecutive microwave irradiation (COOLMATE OPTION 542470-CEM. USA) at 4-10 °C for 4 min. Following centrifugation, the obtained site-specific cross-linked enyzmes (CLEs) were rinsed repeatedly with 1 M NaCl and deionized water for three times. In addition, the cross-linking of two enzymes in an order manner did not end with the formation of dimers, but continued to occur, forming long chains or rings of the two enzymes (**Figure S3**).

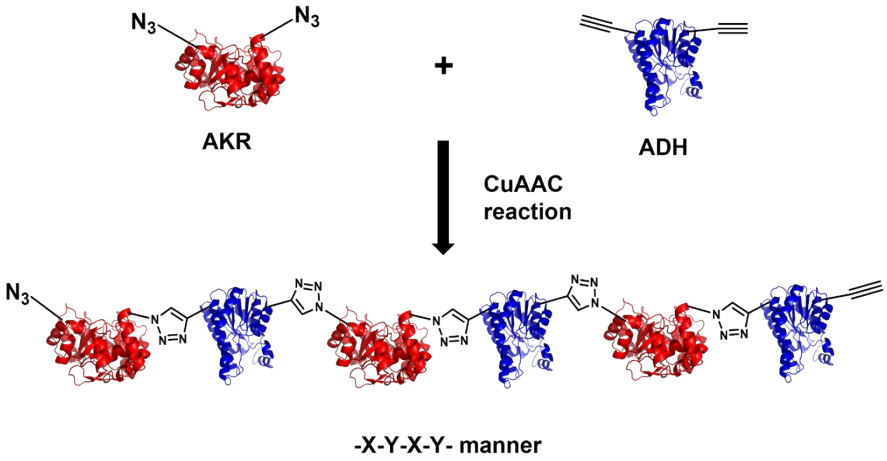

Figure S3. Schematic illustration of O-CLEs

1.3.2 Characterisation of crosslinked enzymes using the supernatants of cell lysates

CLSM

After site-directed mutation of ADH, His-tag at the C-terminus of ADH was replaced by cys-Cys-pro-Gly-Cys-Cys by PCR, and the primers required by PCR were shown in SI. The prepared ordered cross-linked enzymes and site-specific cross-linked enzymes were suspended in TCEP (1 mM) solution, with 1mg of enzyme protein corresponding to 1 mL of reducing agent, and allowed to stand at room temperature for 2.5 h. Then diarseniferin Flash-EDT2 was added until the final concentration was 1mM and stood for 2 h at room temperature. Finally, the second fluorescent staining agent cy5-BisNTA-Ni was added to the final concentration of 1 mM, placed at 4 °C, and incubated for 48 h. After dyeing, add water for centrifugal washing, drop a small amount of sample on the glass slide, and cover the glass slide when slightly dry. The S-CLEs were observed by a laser scanning confocal microscope (Olympus FV 1000 CLSM). Green and red fluorescence were observed in the wavelengths of 577-492 nm and 770-622 nm by CLSM scanning, respectively.

First, a HCCA matrix solution with a concentration of 3 mg/mL (solvent: water-acetonitrile-trifluoroacetic acid = 49:49:2) was prepared at 13,000 g and centrifugated for 5 min. The matrix solution was diluted 500 times and mixed with 1 μL protein solution. Then the 1 μL mixture was placed on the MALDI target plate and dried naturally. Finally, the target plate was put into MALDI mass spectrometer: FlexControl software was turned on to correct method LP_5-20_KDA with protein standard; The sample data was analysed with FlexAnalysis software, and the first-level mass spectrum of the sample was de-noised and smoothen. Using Centroid method, the peak was automatically marked when the SNR was greater than 3, the maximum number of peaks was 100, and the peak width was 5 m/z.

SEM

The cross-linked enzymes were prepared under microwave irradiation and precipitated by centrifugation. After drying, the samples were observed with a scanning electron microscope (JEOL-5600LV), and microscopic images were obtained under a 3.0 kV scanning electron microscope.

FT-IR

The ordered cross-linked enzymes and site-specific cross-linked enzymes were prepared under microwave irradiation and precipitated by centrifugation. And the free enzymes were collected and concentrated in an ultrafiltration tube after they purified by Ni-NTA agarose. Finally, all protein samples were lyophilised and analysed by Fourier Transform Infrared Spectrometer.

MS

To verify the covalent linkage of AKR-ADH ordered cross-linked enzymes and site-specific cross-linked enzymes, the cross-linked enzymes were hydrolysed using 6 M HCl at 110 °C for 24 h in the reactor, and methanol was used as the solvent for MS analysis.

1.3.3 Characterisation of AKR and ADH Ordering in O-CLEs

In order to verify the order of -X-Y-X-Y- structure formed by the alternating connection of AKR and ADH in O-CLEs, we observed O-CLEs by transmission electron microscope (TEM). In order to observe the order of AKR and ADH more clearly, we fused SpyTag at the N-terminal of AKR^{49}_{266} to form SpyTag-AKR^{49}_{266} fusion protein (SpT-AKR^{49}_{266}), and we also constructed SpyCatcher-AKR (SpC-AKR). SpyTag and SpyCatcher can spontaneously form different peptide bonds,[11] so SpC-AKR can be connected with SpT-AKR^{49}_{266}. When SpT-AKR^{49}_{266} was cross-linked with ADH to form O-CLEs, SpC-AKR was added to modify SpT-AKR in O-CLEs to form "-2AKR-ADH-2AKR-ADH-"structure. Then it was observed by TEM.

Table S4. Primers for SpT-AKR^{49}_{266}

Primers	Sequence (5'→3')
SpT-AKR-F1	ATGCTGTACAAAGAACTGGG
SpT-AKR-R1	ACCCAGACTATCCAGCAGTT
SpT-AKR-F2	GATGCCTATAAACCGACCAAAGGTTCAGGGGGTTCCGGTATGCTGTACAAAGAACTGGG
SpT-AKR-R2	ACCCAGACTATCCAGCAGTT
SpT-AKR-F3	GGGGTACCATGGCACATATTGTTATGGTTGATGCCTATAAACCGACCAA
SpT-AKR-R3	CCCAAGCTTTTAGTGATGATGATGATGATGACCCAGACTATCCAGCAGTT

1.4 Regeneration of the cofactor NADPH using $NADP^+$

The cofactor regeneration efficiency was determined by using isopropanol as substrate at 30 °C. The prepared S-CLEs were dissolved in a 1 mL reaction system containing 100 μL $NADP^+$ (2.5 mg/ mL), 100 μL isopropanol (10%) and sodium phosphate buffer (20 mM, pH 8.0). NADPH (mM) produced per minute per milligram S-CLE was determined. The absorbance of NADPH at 340 nm was measured by UV-vis spectrophotometer, and the content of NADPH regenerated using O-CLEs, S-CLEs and CLEAs was calculated. Alcohol dehydrogenase activity was determined by 100 μL $NADP^+$ (2.5 mg/mL), 100 μL isopropanol (10%), 100 μL enzyme solution and 700 mL sodium phosphate buffer (20 mM, pH 8.0).

1.5 Enzyme activity assay

O-CLEs and S-CLEs were obtained by click reaction under consective microwave radiation at 4 °C, and their reducing activity was detected according to previous reports [12]. The reduction activities of O-CLEs and S-CLEs were measured by BECKMAN COULTER Du-730 spectrophotometer. It is important to note that the supernatant should be centrifuged before determining the absorbance. Otherwise, the concentration of enzyme preparations will affect the absorbance of the solution, resulting in a large error in the enzyme activity.

1.6 The apparent Kinetic parameter analysis of cross-linked enzyme

In view of the solubility issue in the aqueous phase, the apparent kinetics of O-CLEAs, S-CLEs and CLEAs were measured by using dihydro-4, 4-dimethyl-2, 3-furandione as a surrogate substrate. The O-CLEAs are ordered cross-linked, thus AKR and ADH contents are certain. However, it is not easy to accurately quantify the specific enzyme proteins within S-CLEs and CLEAs due to their random and disorder crosslinking in cell lysis solution. Hence, the S-CLEs and CLEAs here were prepared using equal amounts of AKR to ADH for the kinetics assays.

We therefore tested the apparent kinetics for O-CLEs, S-CLEs and CLEAs for a crude comparison of catalytic efficiency. The apparent kinetic parameters were obtained at 37 °C using dihydro-4, 4-dimethyl-2, 3-furandione as substrate. The substrate concentration was 0.065 mM to 15.6 mM. The K_M and V_{max} values of O-CLEs, S-CLEs and CLEAs were calculated according to the fitting curve of the relationship between substrate concentration and reaction rate. Changes in the absorbance values of NADPH were detected by UV spectrophotometry at 340 nm and the apparent kinetics were calculated from the consumption of NADPH (**Figure S4**).

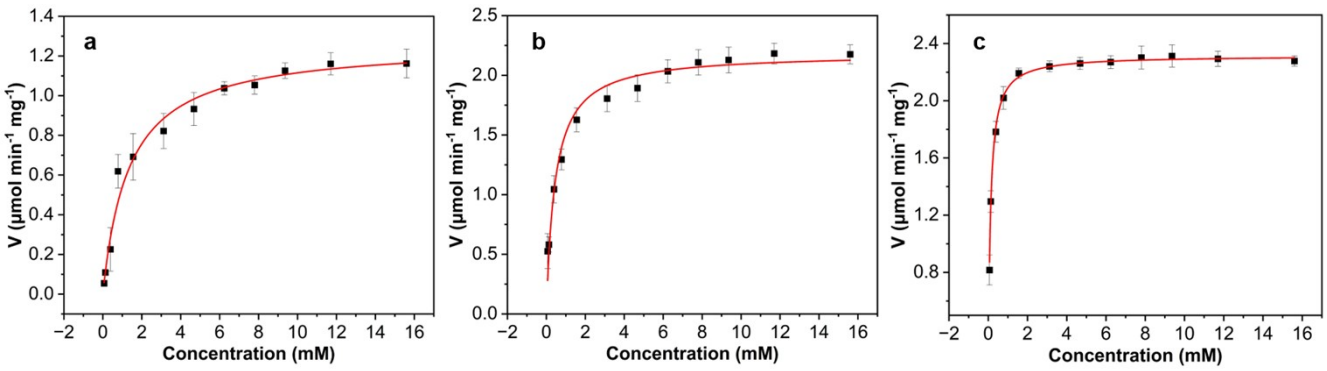

Figure S4. Plots for kinetic parameter determination of *CLEAs* (a), *S-CLEs* (b), and *O-CLEs* (c)

1.7 Enzymatic synthesis of (R)-1-(2-chlorophenyl) ethanol using S-CLEs and CLEAs

O-CLEs were prepared by AKR mutation AKR^{49}_{266}-$2AzF$ containing double *p*-AzF and ADH mutaion ADH^{155}_{189}-$2PaF$ containing double *p*-PaF by self-clicking reaction. S-CLEs prepared by AKR^{49}_{266}-$2AzF$ and ADH mutaion ADH^{155}_{189}-$2AzF$ by SPAAC and CLEAs were prepared using the our previous method [4, 12, 13]. The reaction mixture contains: cross-linked enzyme proteins, 1 mg; 1-(2-chlorophenyl)ethan-1-one, 2 mg; $NADP^+$, 10 mg; isopropyl alcohol, 300 μL; PBS (20 mM, pH 7.0), and the total volume was 2 mL. The reaction was carried out at 30 °C with magnetic stirring for 12 h. Subsequently, insoluble matter was separated by centrifugation and the reaction mixture was extracted with 5 mL n-hexane, and the supernatant was analyzed by HPLC (Agilent 1260). The separation was performed on Daicel IC column (250 mm 4.6 mm, 5 μm particle size). The volume ratio of n-hexane (mobile phase A) to isopropanol (mobile phase B) was 96:4. The flow rate of the pump was 1 mL min^{-1}, the column temperature was maintained at 20 °C, and the injection volume was 10 μL. Data were collected at wavelength 210 nm, and the substrate and target product were verified by the retention time of the corresponding standard. The yield (%) and isomer ratio were calculated according to the standard curve.

The same catalytic system was also used for O-CLEs, S-CLEs and CLEAs turnover frequency (TOF) tests. The reaction took place at 30 °C for 6 h. At the end of each reaction, S-CLE was recycled by centrifugation and put into the next cycle of catalysis. The cycle was 5 times, and the substrate conversion amount of each time was measured by HPLC. Generally, the turnover frequency (TOF) [14-16] is defined as the number of catalytic reactions or the number of target products formed or reactants consumed per unit time at the active site.

TOF and TON are calculated as follows, [14]

$$TOF = Number\ of\ catalytic\ events/(Time * Number\ of\ active\ sites)$$

$$TON = Amount\ of\ product/(Amount\ of\ catalyst)$$

When examing the conversion, the total volume of reaction system was 10 mL. It consisted of enzyme, 1 mg; 1-(2-chlorophenyl)ethan-1-one, 10 mg; $NADP^+$, 50 mg; isopropyl alcohol, 1.5 mL; and PBS (20 mM, pH 7.0) was added to 10 mL. The reaction was carried out at 30 °C with magnetic agitation. Samples were taken every 2 hours until 24 hours after the start of the reaction. 800 μL of reaction liquid was extracted each time, centrifugal extraction, liquid phase detection, and substrate conversion was calculated according to the standard curve.

1.8 The cross-linked protein-protein complexes predicted by ZDOCK

The structure of the cross-linked enzyme complexes was predicted by the ZDOCK module of Discovery Studio Client (V4), which is a rigid protein-protein docking algorithm using a 3-dimensional (3D) fast Fourier transform (FFT). The structures of AKR and ADH were uploaded as the receptor protein and ligand protein, respectively. Receptor binding site residues included Glys153, Ala154 and Tyr155. Ligand binding site residues included Glu265, Glu266, Met267 and Lys268. Other parameters were set to default values, as shown in **Table 1**. After the calculation was completed, 2000 possible interaction conformations of dimer were obtained with different ZDock Score and ZRank Score. The appropriate conformations were selected based on the orientation of co-enzyme channeling and the distance of two active pockets (≤15 Å). Furthermore, the trimeric structure was predicted using the similar protocol with modifications. The selected conformation of dimer was inputted as the receptor protein, and ADH was used as the ligand protein. Receptor binding site residues included Gly48, Tyr49 and Thr50. Ligand binding site residues included Gly188, Tyr189 and Ile190. The hexamer was obtained by analogy.

Table S5. The protein-protein docking parameters of AKR and ADH

Parameter name	***Parameter value***
Input receptor protein	ADH
Input ligand protein	AKR
Angular step size	6
Receptor binding site residues	Gly153, Ala154, Tyr155
Ligand binding site residues	Glu265, Glu266, Met267, Lys268
Distance cutoff	10
Top poses	2000
RMSD cutoff	10
Interface cutoff	10
Maximum number of clusters	60

2. Results and Discussion

2.1 SDS-PAGE and MALDI-TOF-MS analysis of AKR and ADH mutants

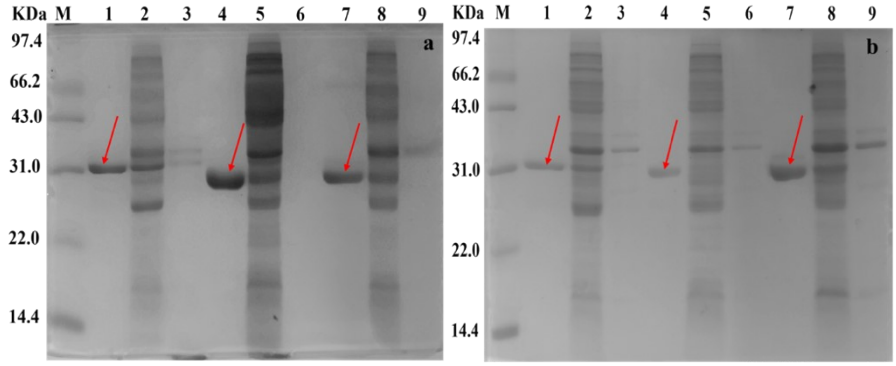

Figure S5. SDS-PAGE analysis of AKR and ADH mutants: (a) (M, Marker; Line 1, purified AKR^{138}_{215}-$2AzF$; Line 2, supernatant of cell lysate; Line 3, insoluble in cell lysate. Line 4, purified ADH^{3}_{251}-$2PaF$; Line 5, supernatant of cell lysate; Line 6, insoluble in cell lysate. Line 7, purified ADH^{3}_{251}-$2AzF$; Line 8, supernatant of cell lysate; Line 9, insoluble in cell lysate), (b) (M, Marker; Line 1, purified AKR^{49}_{266}-$2AzF$; Line 2, supernatant of cell lysate; Line 3, insoluble in cell lysate. Line 4, purified ADH^{155}_{189}-$2PaF$; Line 5, supernatant of cell lysate; Line 6, insoluble in cell lysate. Line 7, purified ADH^{155}_{189}-$2AzF$; Line 8, supernatant of cell lysate; Line 9, insoluble in cell lysate)

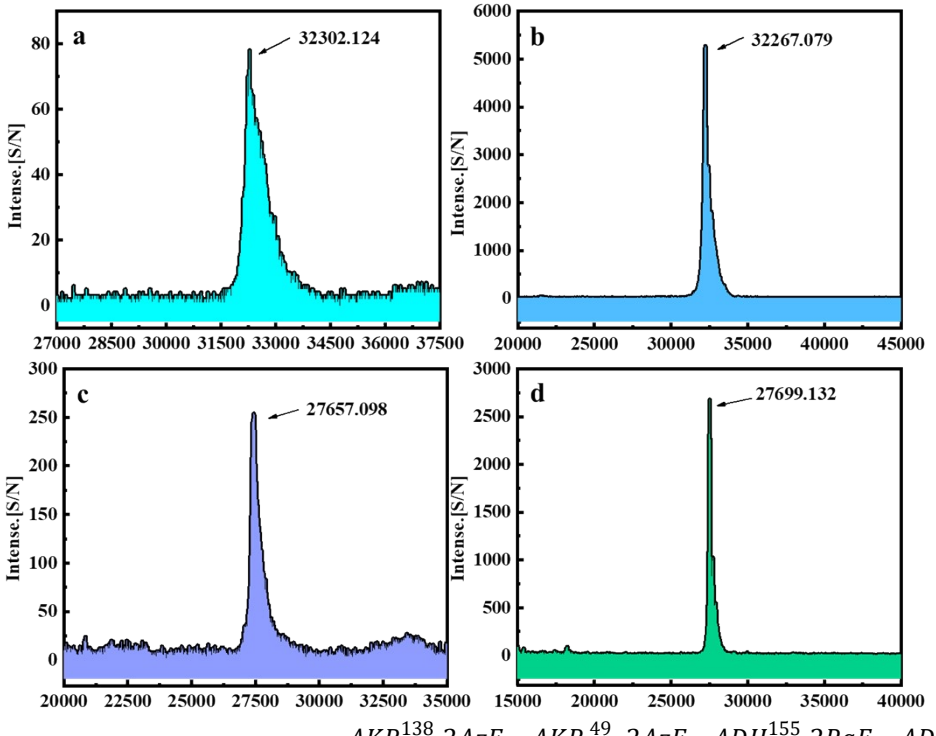

Figure S6. MALDI-TOF-MS analysis of AKR and ADH mutants. (a, AKR^{138}_{215}-$2AzF$; b, AKR^{49}_{266}-$2AzF$; c, ADH^{155}_{189}-$2PaF$; d, ADH^{3}_{251}-$2PaF$)

2.2 Morphology characterization of ordered crosslinked and fixed-point crosslinked S-CLEs

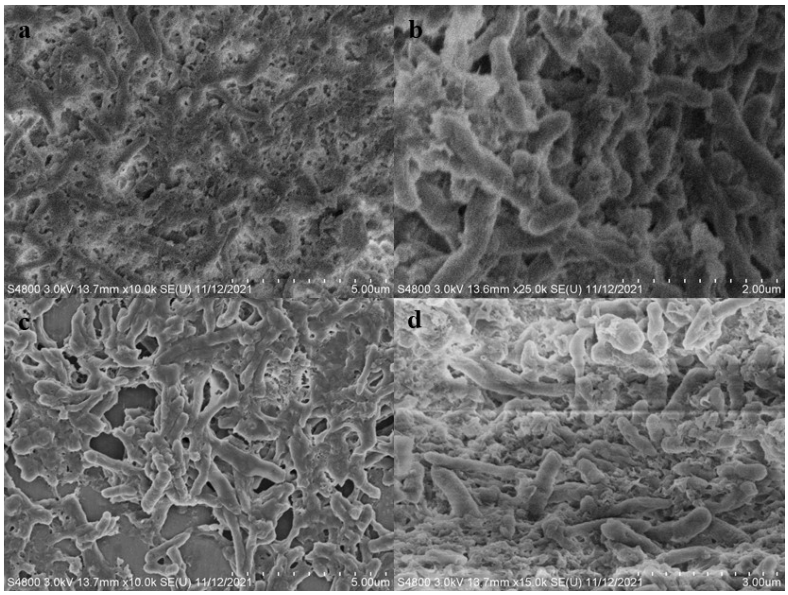

Figure S7. SEM scanning of S-CLEs and O-CLEs (a, S-CLEs of AKR^{49}_{266}-$2AzF$ and ADH^{155}_{189}-$2AzF$; b, O-CLEs of AKR^{49}_{266}-$2AzF$ and ADH^{155}_{189}-$2PaF$; c, S-CLEs of AKR^{138}_{215}-$2AzF$ and ADH^{155}_{189}-$2AzF$; d, O-CLEs of AKR^{138}_{215}-$2AzF$ and ADH^{155}_{189}-$2PaF$)

The prepared S-CLEs containing AKR and ADH mutants can be discriminated by scanning electron microscope (**Figure S7**). However, AKR and ADH in S-CLEs can not be distinguished by scanning electron microscope, or even transmission electron microscope (TEM) and atomic force microscope (AFM). So, how to determine which is O-CLEs and which is S-CLEs? As shown in **Figure S2**, in O-CLES two AKR are linked with a ADH as -AKR-ADH-AKR-ADH- (**Figure S2C**) and both enzymes are uniformly cross-linked. However, in site-specific cross-linked enzymes (S-CLEs), because both enzyme mutants contain just *p*-AzF and are cross-linked using the added cyclooctyne, cross-linking can occur to all enzymes in the supernatant of cell lysates. This means no uniformity and succession in S-CLEs even if site-specific covalent linkage can be ensured (**Figure S2B**).

To further confirm the cross-linking of the two enzymes, a labeling strategy using a short peptide tag and a complementary recognition pair of small molecular probes was introduced [17].

Histidine tags (HIS-Tags) were originally developed as affinity tags for protein purification, but have also been applied to selective protein labeling. A routine combination of His tag and nitrotriacetic acid (NTA) -Ni probes is a simple and sensitive method for labeling proteins [18]. Because his-Tag can also be used in protein purification operations, which is the tag added to the enzyme protein in this experiment, the protein labeling method using Cy5-BisNTA-Ni specifically combining his-Tag is the first choice. Secondly, the short peptide sequence Cys-Cys-XaA-xAA-Cys-Cys, where Xaa is a non-cysteine amino acid that is genetically fused or inserted into the protein, can be specifically recognised by FlAsH, a transmembrane luciferin derivative with two As (III), which fluoresces only after arsenic is bound to cysteine thiol [19]. Therefore, flash-EDT2 combined with cysteine (CCXXCC) labeling method was also used in this study.

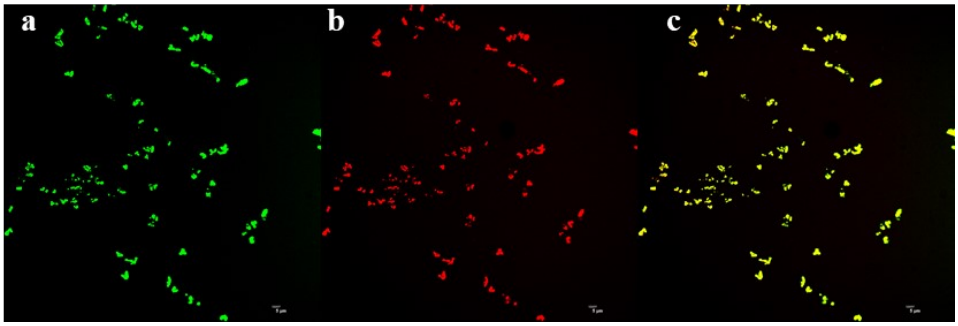

Figure S8. CLSM images of O-CLEs of AKR^{138}_{215} and ADH^{155}_{189}

After O-CLEs and S-CLEs were obtained, two fluorescent probes were added together, in which AKR mutant-His-Tag specifically bound to Cy5-Bisnta-Ni, and ADH mutant-Cys-Cys-pro-Gly-Cys-Cys bound to Flash-EDT2. It was scanned by CLSM, and red fluorescence was observed in the wavelength range of 770-622 nm for AKR mutants, while green fluorescence was observed in the wavelength range of 577-492 nm for ADH mutants in **Figure S8**. Can be seen in the graph, presented O-CLEs fluorescent red and green fluorescence pattern

is consistent, and in the full wavelength combination figure can see yellow color uniform design consistent image, can be in O-CLEs AKR mutants and ADH mutant cross-linking is orderly cross connection, so that they emit almost composite fluorescence pattern.

However, in S-CLEs, disordered cross-linking of two enzymes could be observed. The red fluorescence pattern of AKR-mutants was obviously different from the green fluorescence pattern of ADH-mutants, and the effect of random cross-linking was more obvious in the full-wavelength combination pattern. There were obvious aggregation of AKR red fluorescence and obvious aggregation of ADH green fluorescence, of course, even cross-linking was one of them (**Figure S9**).

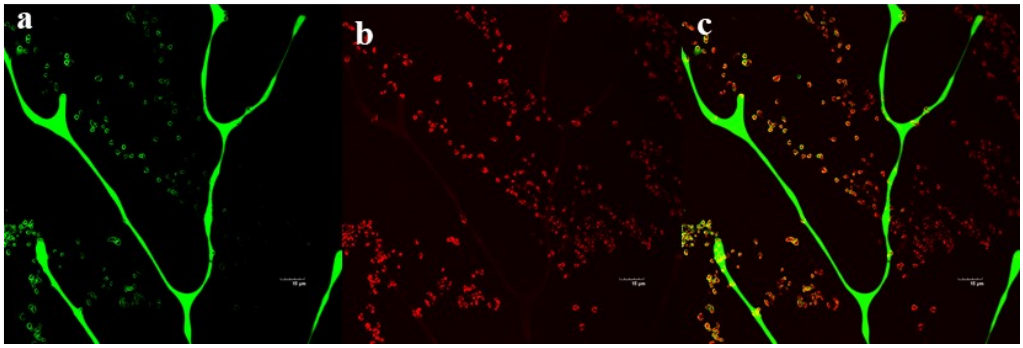

Figure S9. CLSM images of S-CLEs of AKR^{138}_{215} and ADH^{155}_{189}

2.3 Structural demonstration of crosslinking enzyme

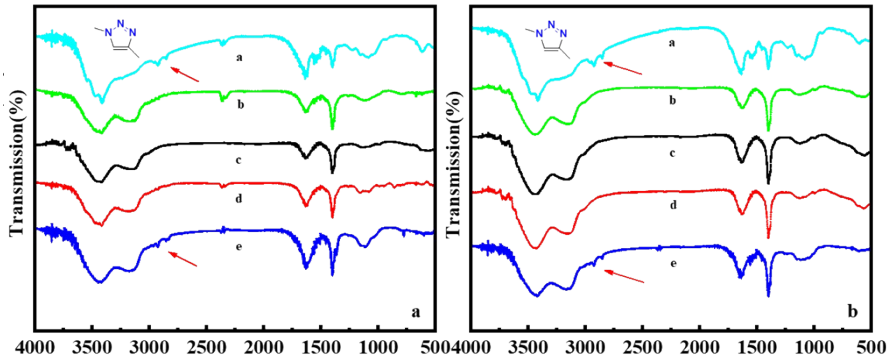

Figure S10. FT-IR analysis of O-CLEs, S-CLEs and purified enzyme mutants (a) S-CLEs of AKR^{138}_{215} and ADH^{3}_{251} (b) a, O-CLEs of AKR^{49}_{266} and ADH^{155}_{189}; b, ADH^{155}_{189}; c, AKR^{49}_{266}; d, ADH^{3}_{251}; e, S-CLEs of AKR^{138}_{215}- ADH^{3}_{251}; c: AKR^{138}_{215}, ADH^{3}_{251}; d, AKR^{49}_{266} and ADH^{155}_{189})

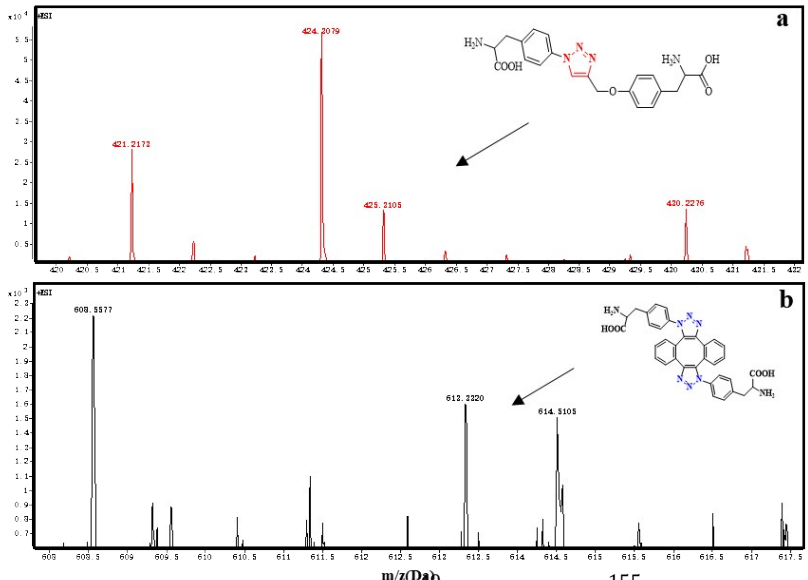

Figure S11. MS analysis of O-CLEs and S-CLEs after acidolysis (a, O-CLEs of AKR^{49}_{266}-$2AzF$ and ADH^{155}_{189}-$2PaF$; b, S-CLEs of AKR^{49}_{266}-$2AzF$ and ADH^{155}_{189}-$2AzF$)

2.4 TGA analysis of the obtained CLEAs and S-CLEs

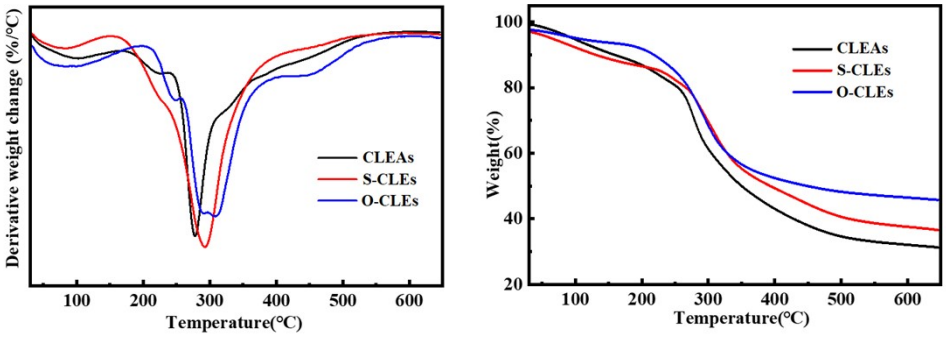

Figure S12. TGA analysis of the obtained carrier-free immobilized AKR and ADH mutants

2.5 TEM characterization of O-CLEs

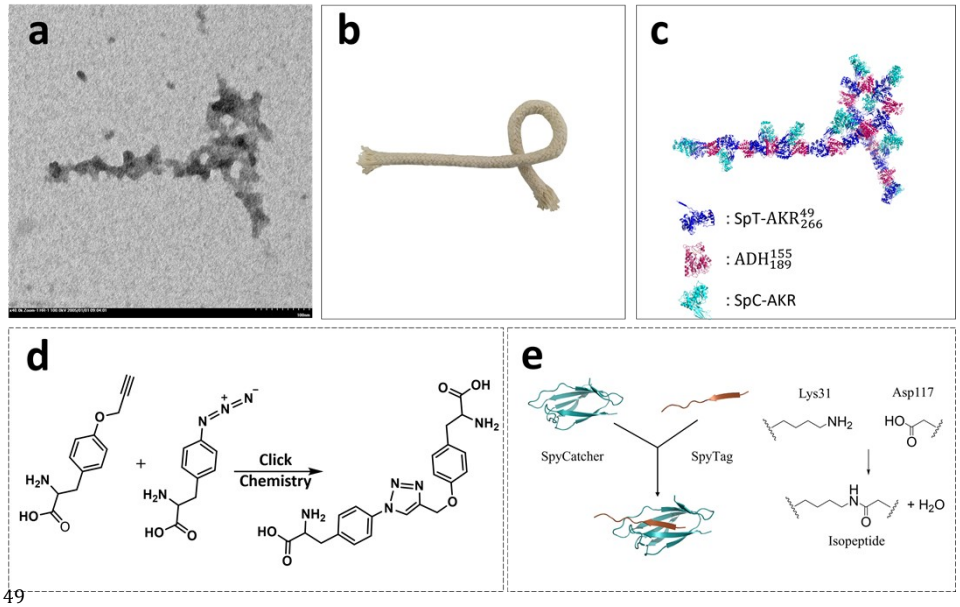

Figure S13. SpT-AKR^{49}_{266} and ADH^{155}_{189} in O-CLEs was modified by the fusion protein SpC-AKR through the spontaneous reaction between SpyTag and SpyCatcher, and then the order of AKR^{49}_{266} and ADH^{155}_{189} was observed by TEM (a, TEM images of O-CLEs; b, S-CLEs wrapped like ropes; c, Protein schematic diagram; d, Specific click chemistry reaction between AKR^{49}_{266} and ADH^{155}_{189}; e, Reaction between SpyTag and SpyCatcher)

To verify the order of AKR and ADH on O-CLEs, a SpyTag/SpyCatcher system was employed to increase the identification of CLEs under transmission electron microscopy (TEM) by fusing another protein at one of its protein components. First, a SpyTag (SpT) was fused at N-terminals of AKR^{49}_{266} of O-CLEs, and a SpyCatcher (SpC) was fused at N terminal of wild AKR. They were subsequently mixed to form the new CLEs via the specific coupling of SpyCatcher and SpyTag. As shown in **Figure S13**, the bulgy protein in the new CLEs verified the success bio-orthogonal connection of SpT-AKR^{49}_{266} with SpC-AKR. This demonstrates the formation of O-CLEs in -X(X)-Y-X(X)-Y- manner, and further indicates that the order of AKR^{49}_{266} and ADH^{155}_{189} in the dual enzyme O-CLEs as -X-Y-X-Y- manner.

2.5 Cofactor regeneration efficiency and reducing activity of crosslinked enzyme

The enzyme aggregate obtained by cross-linking at different sites was tested, and the cross-linking modes of each site were divided into ordered, site-specific and random cross-linking. Comparative analysis was conducted in terms of cofactor regeneration efficiency and reducing activity, as shown in **Figure S14**. In comparative analysis, the enzyme aggregates prepared by ordered crosslinking method (O-CLEs) showed better reducing activity and higher NADPH production rate than those prepared by fixed point crosslinking (S-CLEs) and random cross-linking (CLEAs). In general, in the co-fixation system with multiple enzyme combinations, the cofactor regeneration rate is much higher than that in the free diffusion system, and the cofactor regeneration efficiency increases with the decrease of the distance between enzymes [20]. The initial production rate of of NADPH using ADH in the enzyme aggregates can be used as a measure of the efficiency of the cascade reaction [21, 22].

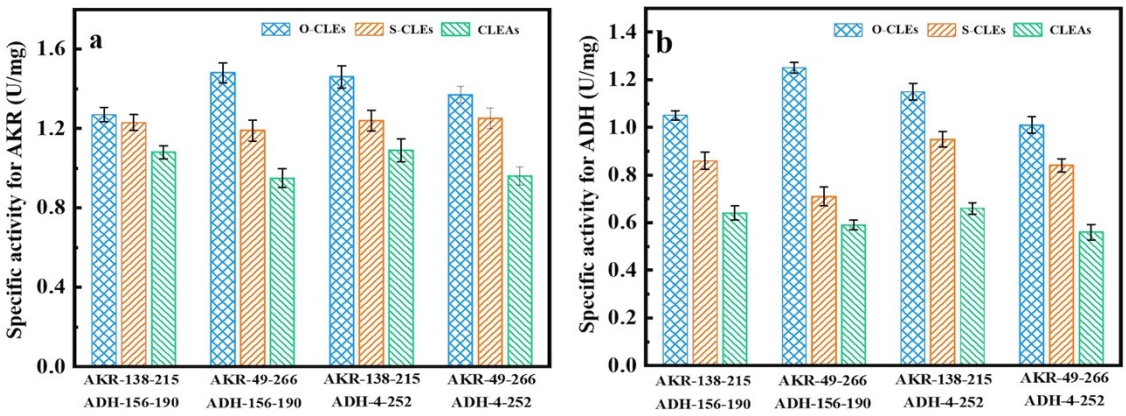

Figure S14. NADPH reducing and generating activity of O-CLEs, S-CLEs and CLEAs. (a, NADPH reducing; b, NADPH generating)

2.6 Crosslinked enzyme catalysed synthesis of (R)-1-(2-chlorophenyl) ethanol

Because of higher specific activity, O-CLEs of AKR^{49}_{266}-$2AzF$ and ADH^{155}_{189}-$2PaF$, S-CLEs of AKR^{49}_{266}-$2AzF$ and ADH^{155}_{189}-$2AzF$ and CLEAs were used to catalyse the synthesis of (R)-1-(2-chlorophenyl) ethanol to examine their catalytic performance in the cascade reaction. Figure 3-B shows that the yield of the target product catalysed by O-CLEs is 96.70%, which is higher than that of S-CLEs and CLEAs. In the catalysed synthesis products, the ee value was 99.99%, and HPLC analysis showed that (S)-1-(2-chlorophenyl) ethanol had no obvious peak (**Figure S, 4 h-24 h**). In S-CLEs, site-directed cross-linking of the enzyme is more targeted than random cross-linking (CLEAs), which helps to retain the original conformation and activity of the enzyme protein to the maximum extent. This may contribute to achieving higher catalytic activity in catalytic reactions than with random cross-linked enzyme aggregates [23]. In addition, the simplified one-step preparation of S-CLEs from cell crushing supernatant preserved the enzyme activity to a greater extent [24]. The catalytic yield of O-CLEs is higher than that of S-CLEs, because in the cascade reaction, ordered cross-linking is more favorable than disordered fixation. The ordered multi-enzyme cascade system is easier to exchange intermediates between active sites and reduce the loss of unstable intermediates or cofactors [25]. In addition, it may be related to the distance between enzymes and the substrate channel effect, which shows that the catalytic activity increases with the decrease in distance [20].

Compared with CLEAs, both O-CLEs and S-CLEs showed high activity and selectivity in the catalytic reaction with suitable substrate concentration, indicating the feasibility of using click chemical cross-linking method for non-natural amino acid insertion of enzyme protein. In the conversion detection of cascade catalysis, adding five times the amount of substrate, under the same system and conditions, the relationship diagram of O-CLEs, S-CLEs and CLEAs substrate conversion with time was obtained. It can be seen from **Figure S** that the initial catalytic efficiency of O-CLEs is much higher than that of S-CLEs and CLEAs, and the conversion rate rapidly reaches 93.1% after 14 h of reaction, and finally reaches 96.7%. However, the conversion rates of S-CLEs and CLEAs were 54.8% and 15.9% at 14 h, and finally reached 74.4% and 25.8 %. At 14 h, the substrate conversion rate of O-CLEs is 1.69 times that of S-CLEs and 5.85 times that of CLEAs, showing high catalytic efficiency in the cascade reaction.

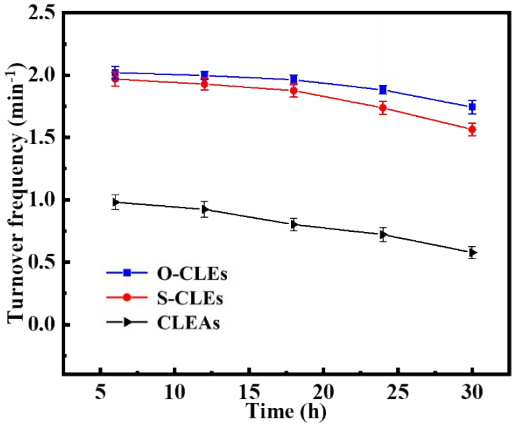

Figure S15. Conversion change diagram of (R)-1-(2-chlorophenyl) ethanol catalyzed by O-CLEs, S-CLEs and CLEAs; Diagram of change in turnover frequency (TOF) in cyclic catalysis

In order to further detect the change of catalytic performance of O-CLEs and S-CLEs in the cascade reaction, the turnover frequency (TOF) of O-CLEs and S-CLEs in the cascade catalytic system was determined in the continuous catalysis of 30 h (**Figure S15**). It can be clearly seen from B in **Figure S15** that the decline in TOF value of O-CLEs (2.02 to 1.75) is less than that of S-CLEs (1.96 to 1.5) and CLEAs (0.98 to 0.57), indicating that O-CLEs has higher stability than S-CLEs and CLEAs in the continuous catalytic process. Therefore, it can be speculated that this is because the protein aggregation formed by orderly cross-linking can better remain highly active. The TOF value of O-CLEs was

always higher than that of S-CLEs, which might be because TOF decreased with increasing distance between enzymes [20]. However, due to the complicated purification process and non-specific covalent linking, the catalytic performance of random cross-linking enzyme aggregates (CLEAs) decreases [26-28].

2.7 HPLC analysis of the yielded chiral alcohol in the catalysis using CLEAs and S-CLEs of AKR and ADH

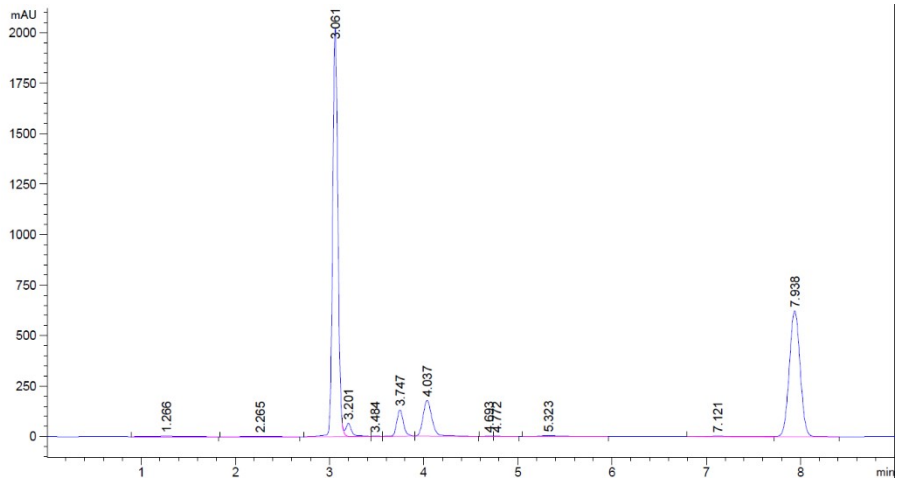

Figure S16. Normal phase HPLC of the substrate. The pump runs at a flow rate of 1 mL·min^{-1}; Solvent A is n-hexane; solvent B is isopropanol; The volume ratio of n-hexane to isopropanol is 98:2 (v/v); The data was collected at 210 nm and the injection volume is 10 µL each time.

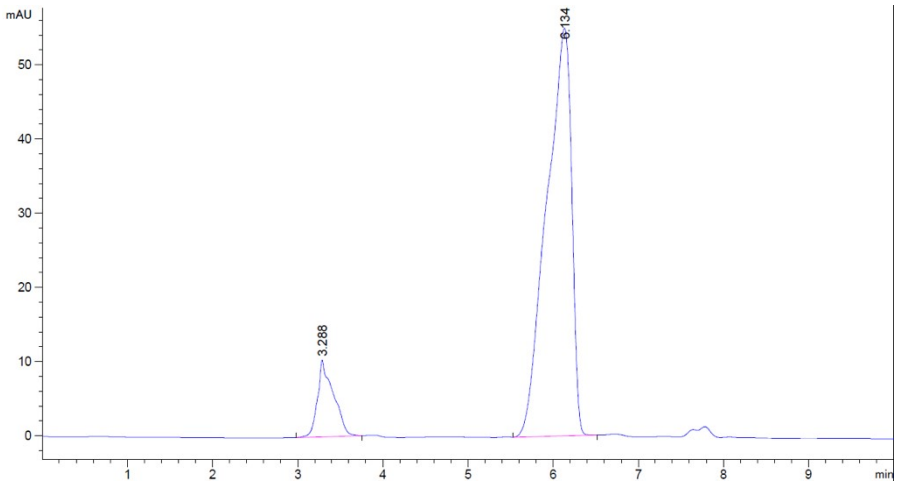

Figure S17. Normal phase HPLC of (R)-1-(2-chlorophenyl)ethanol. The pump runs at a flow rate of 1 mL·min^{-1}; Solvent A is n-hexane; solvent B is isopropanol; The volume ratio of n-hexane to isopropanol is 98:2 (v/v); The data was collected at 210 nm and the injection volume is 10 µL each time.

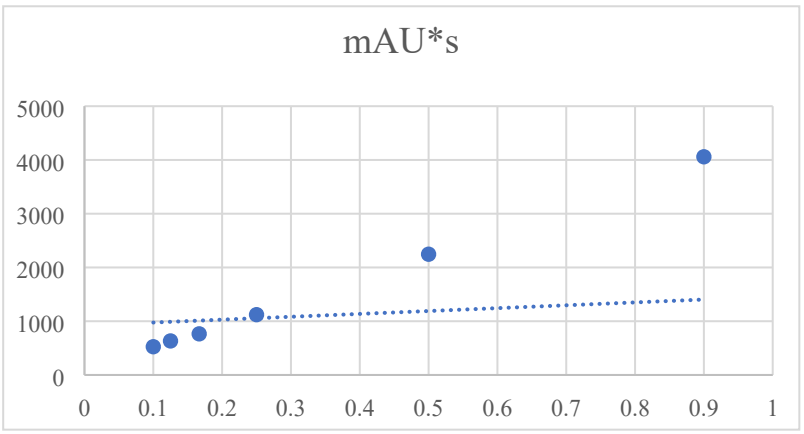

Figure S18. Standard curve for normal phase HPLC of (R)-1-(2-chlorophenyl)ethanol. The pump runs at a flow rate of 1 mL·min^{-1}; Solvent A is n-hexane; solvent B is isopropanol; The volume ratio of n-hexane to isopropanol is 98:2 (v/v); The data was collected at 210 nm and the injection volume is 10 μL each time.

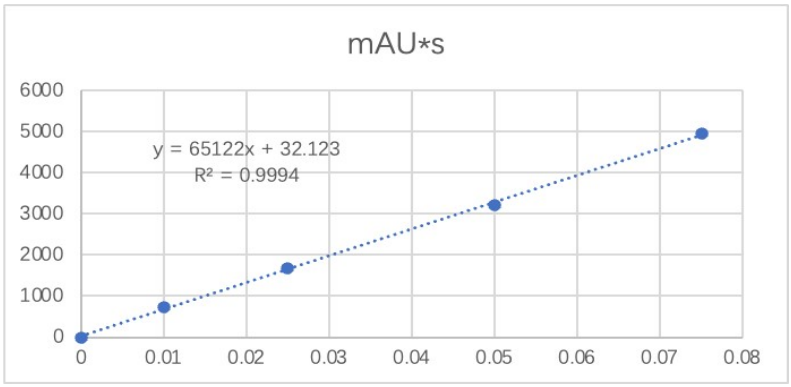

Figure S19. Standard curve for normal phase HPLC of o-chloroacetophenone.The pump runs at a flow rate of 1 mL·min^{-1}; Solvent A is n-hexane; solvent B is isopropanol; The volume ratio of n-hexane to isopropanol is 98:2 (v/v); The data was collected at 210 nm and the injection volume is 10 μL each time.

HPLC analysis of the yielded chiral alcohol in different reaction time using carrier-free immobilized dual enzyme of AKR and ADH

Crosslinked enzyme aggregates (CLEAs): **Figure S** (CLEAs, 4 h-24 h)

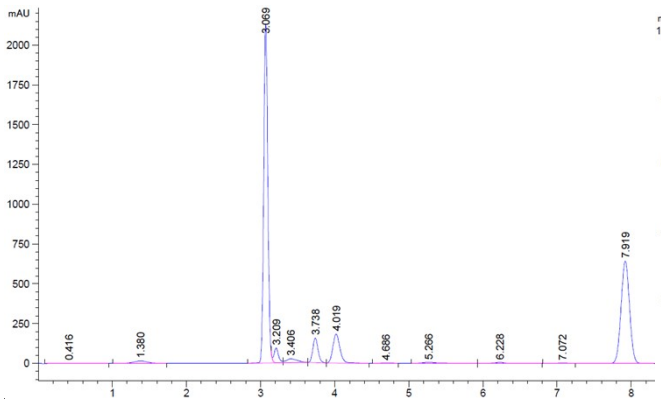

CLEAs: 4 h

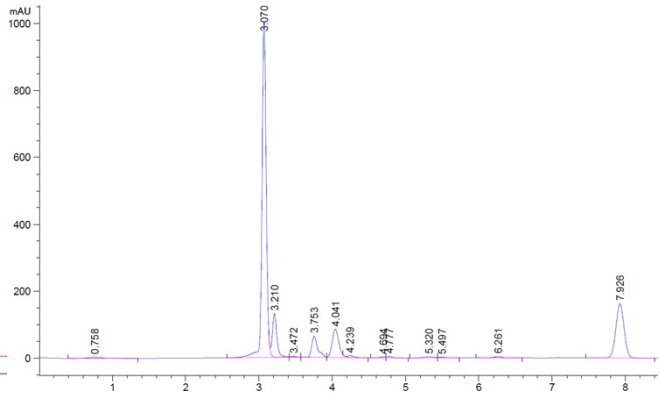

CLEAs: 6 h

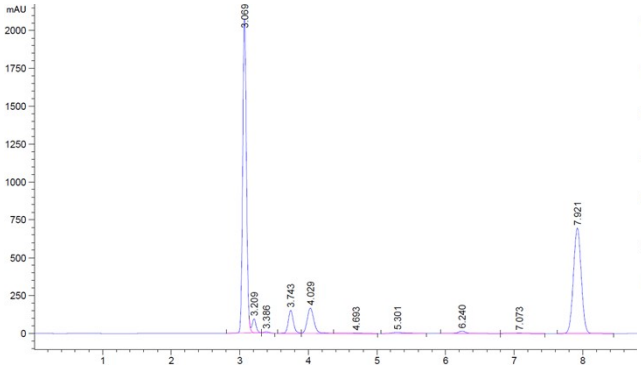

CLEAs: 8 h

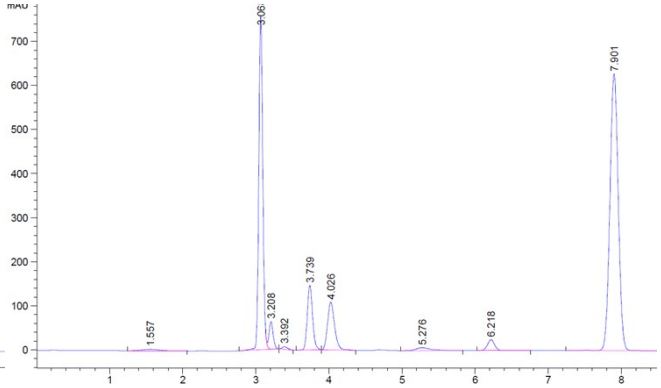

CLEAs: 10 h

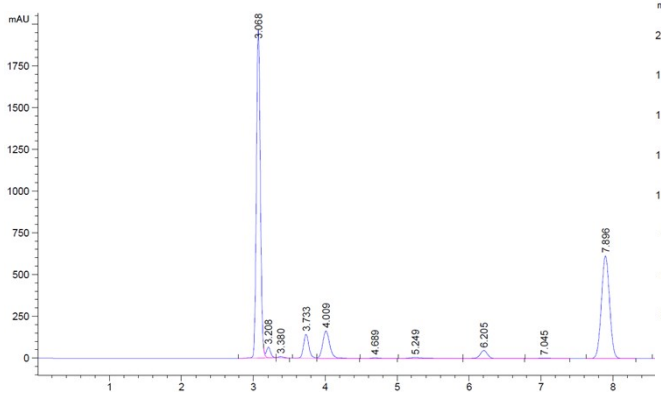

CLEAs: 12 h

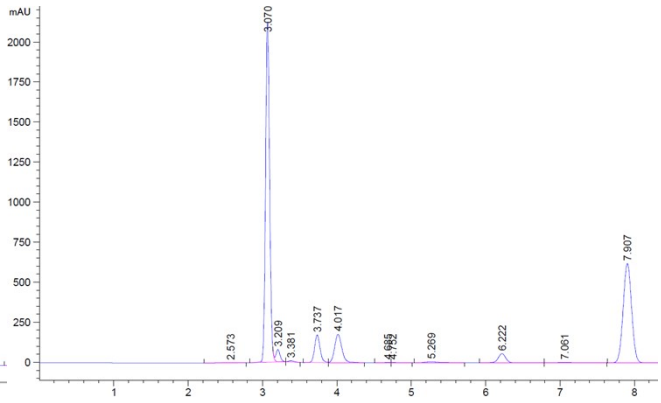

CLEAs: 14 h

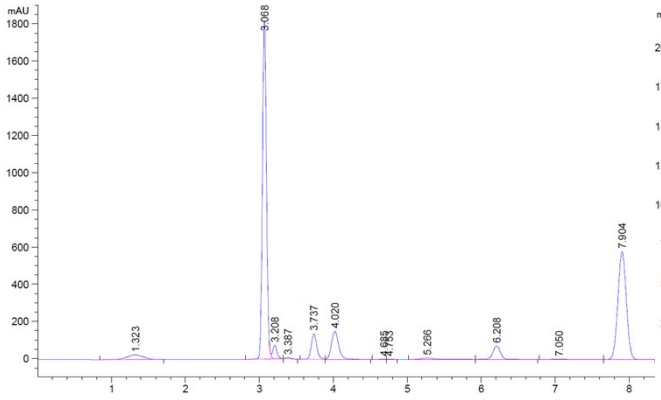

CLEAs: 18 h

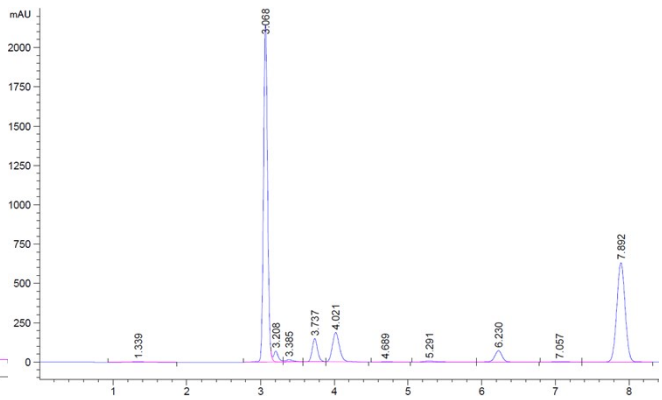

CLEAs: 22 h

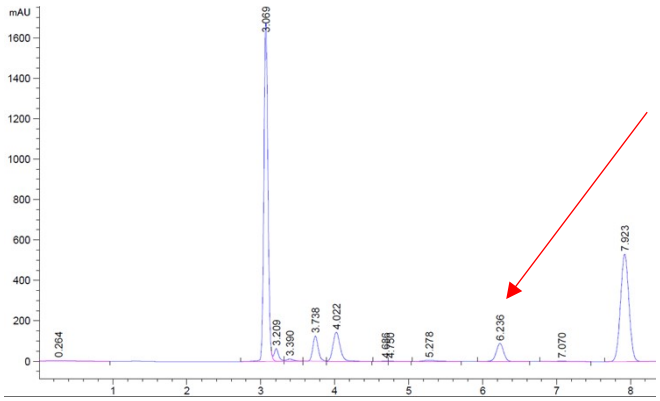

CLEAs: 24 h

Site-specific crosslinked enzymes (S-CLEs) of AKR^{49}_{266}-$2AzF$ ***and*** ADH^{155}_{189}-$2AzF$:

Figure S (S-CLEs, 4 h-24 h)

S-CLEs: 4 h

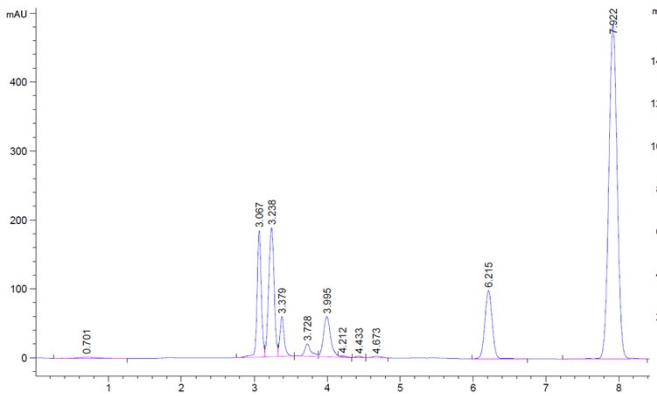

S-CLEs: 6 h

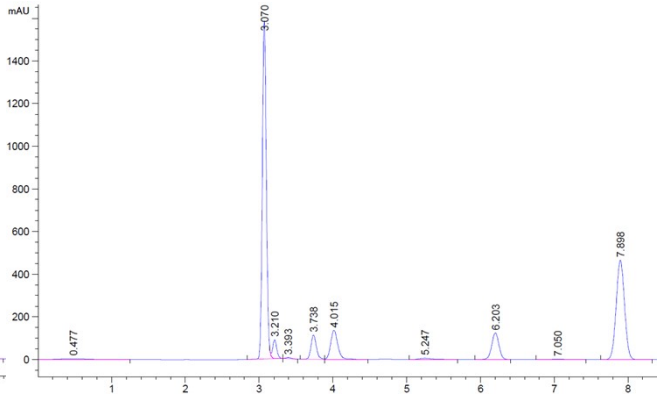

S-CLEs: 8 h

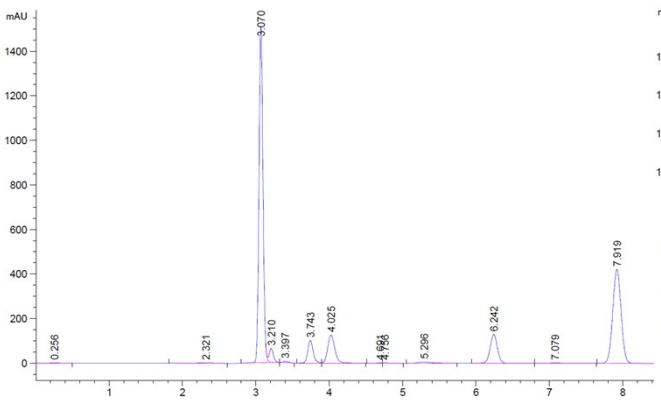

S-CLEs: 10 h

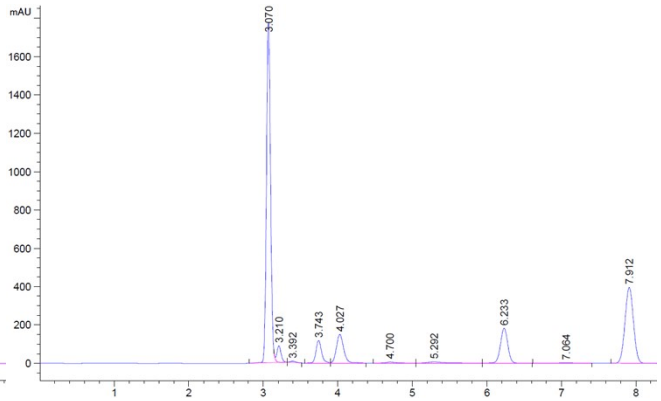

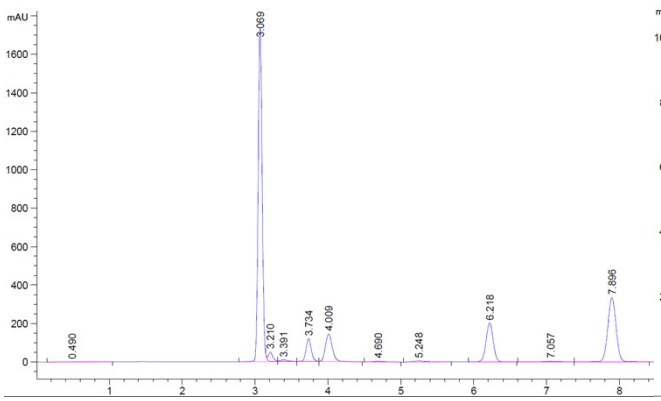

S-CLEs: 12 h

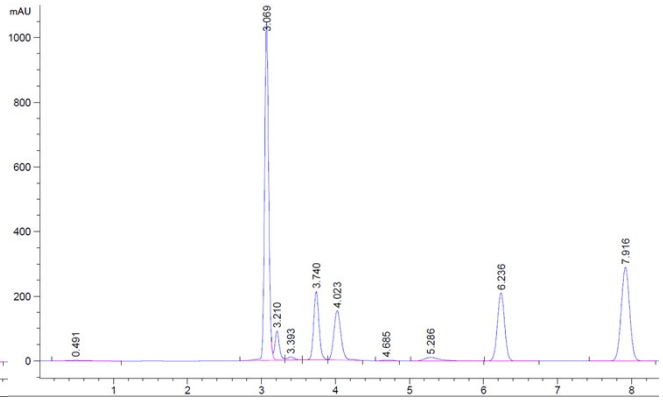

S-CLEs: 14 h

S-CLEs: 18 h

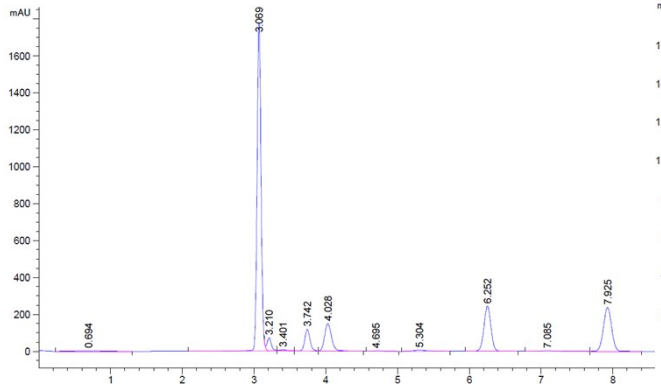

S-CLEs: 22 h

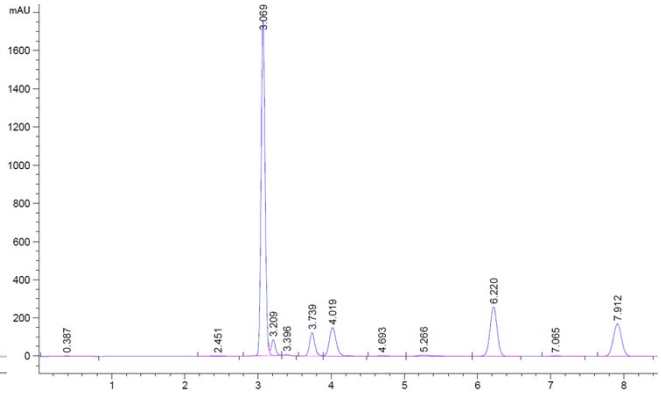

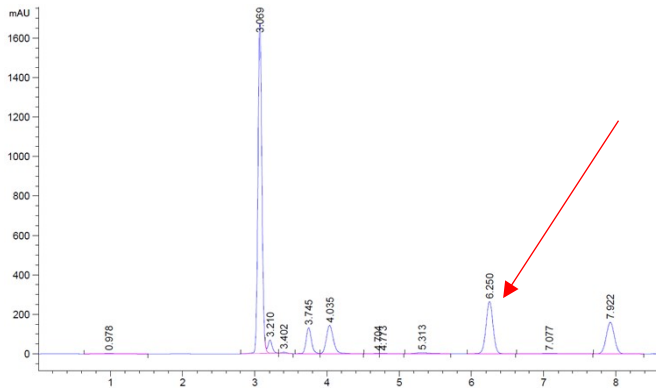

S-CLEs: 24 h

Orderly crosslinked enzymes (O-CLEs): O-CLEs of $AKR^{49}_{266}$and ADH^{155}_{189}

Figure S (O-CLEs, 4 h-24 h)

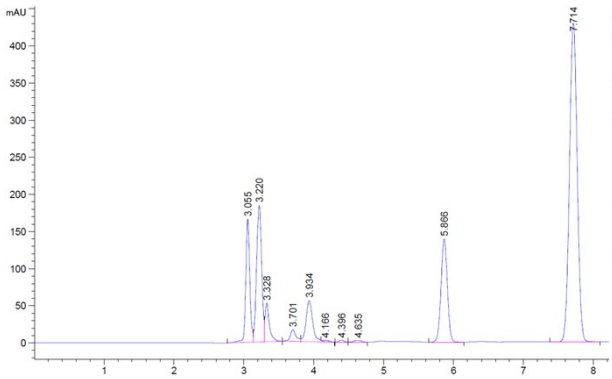

O-CLEs: 4 h

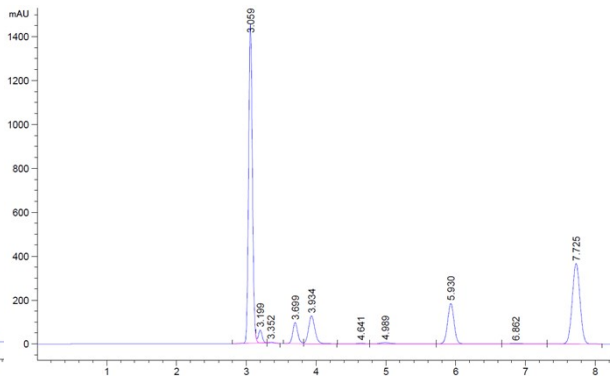

O-CLEs: 6 h

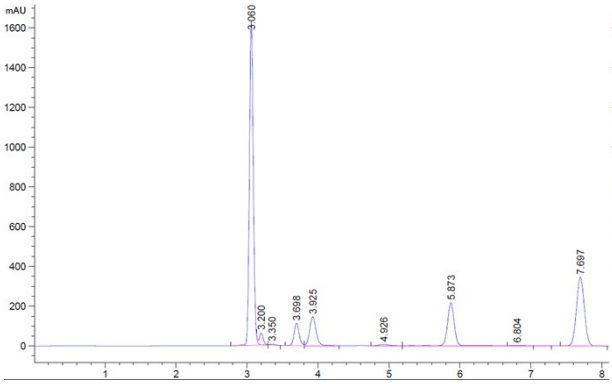

O-CLEs: 8 h

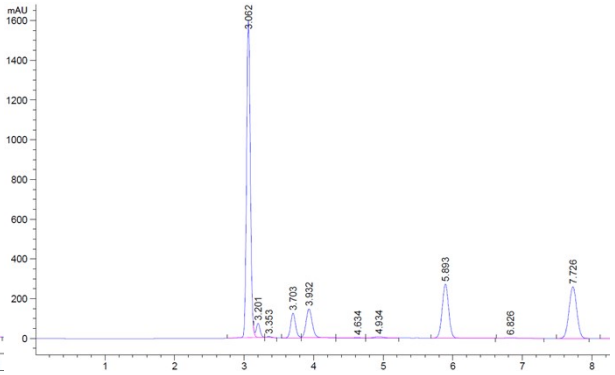

O-CLEs: 10 h

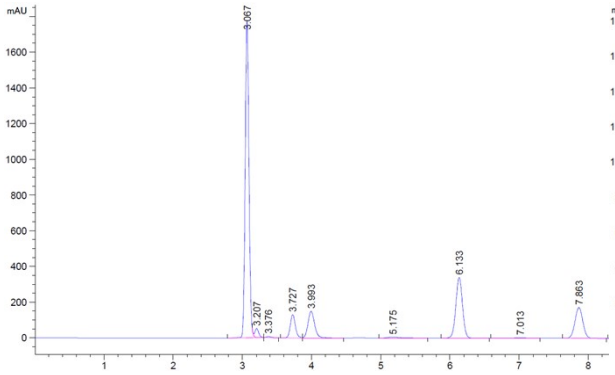

O-CLEs: 12 h

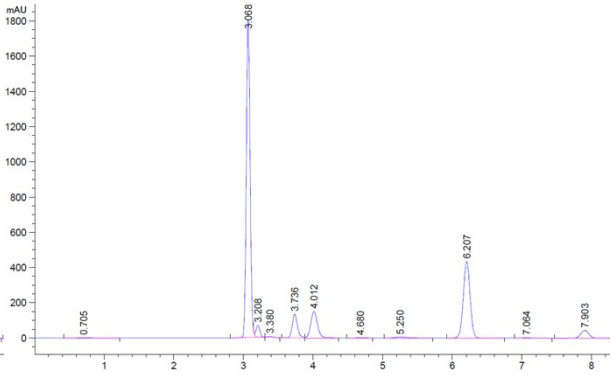

O-CLEs: 14 h

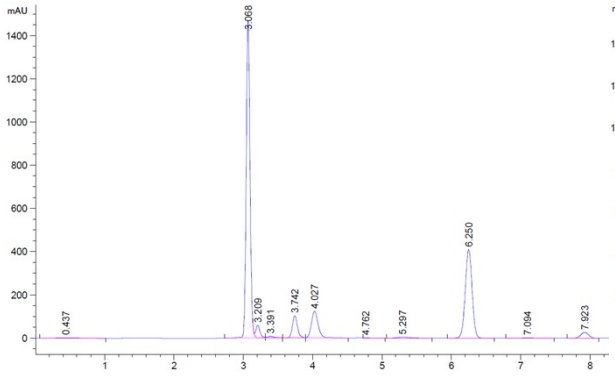

O-CLEs: 18 h

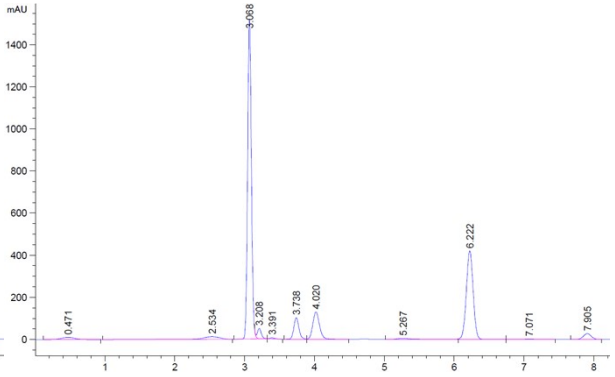

O-CLEs: 22 h

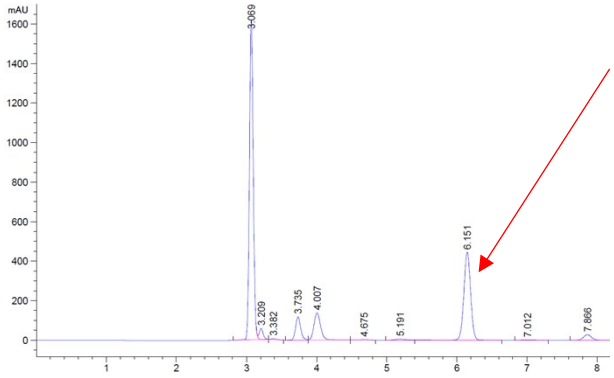

O-CLEs: 24 h

2.8 ZDOCK of the protein-protein interaction in O-CLEs of AKR and ADH

Table S6 The protein-protein docking results of top 30 conformations

Poses	Density	Cluster size	ZDock Score	ZRank Score
Pose1	12	36	15	-84.914
Pose2	13	18	12.68	-79.285
Pose3	75	85	13.72	-78.977
Pose4	25	14	13.8	-78.864
Pose5	13	36	12.46	-77.425
Pose6	40	43	12.5	-75.741
Pose7	13	36	13.46	-74.824
Pose8	10	10	11.58	-74.649
Pose9	54	62	14.94	-74.357
Pose10	15	36	11.3	-73.973
Pose11	29	54	11.78	-73.86
Pose12	48	54	11.94	-72.096
Pose13	21	37	11.46	-71.901
Pose14	66	85	13.7	-71.607
Pose15	57	62	13.38	-71.591
Pose16	70	85	13.36	-71.264
Pose17	26	29	14.78	-70.35
Pose18	57	62	15.24	-69.882
Pose19	9	36	12.16	-69.289
Pose20	65	85	13.16	-68.266
Pose21	56	62	16.12	-68.191
Pose22	41	46	15.74	-68.151
Pose23	73	85	13.4	-67.827
Pose24	72	80	14.2	-67.819
Pose25	50	54	12.2	-67.739
Pose26	13	18	14.08	-67.646
Pose27	53	85	12.88	-67.501
Pose28	6	1	11.62	-67.081
Pose29	70	62	11.84	-66.759
Pose30	13	8	12.14	-66.708

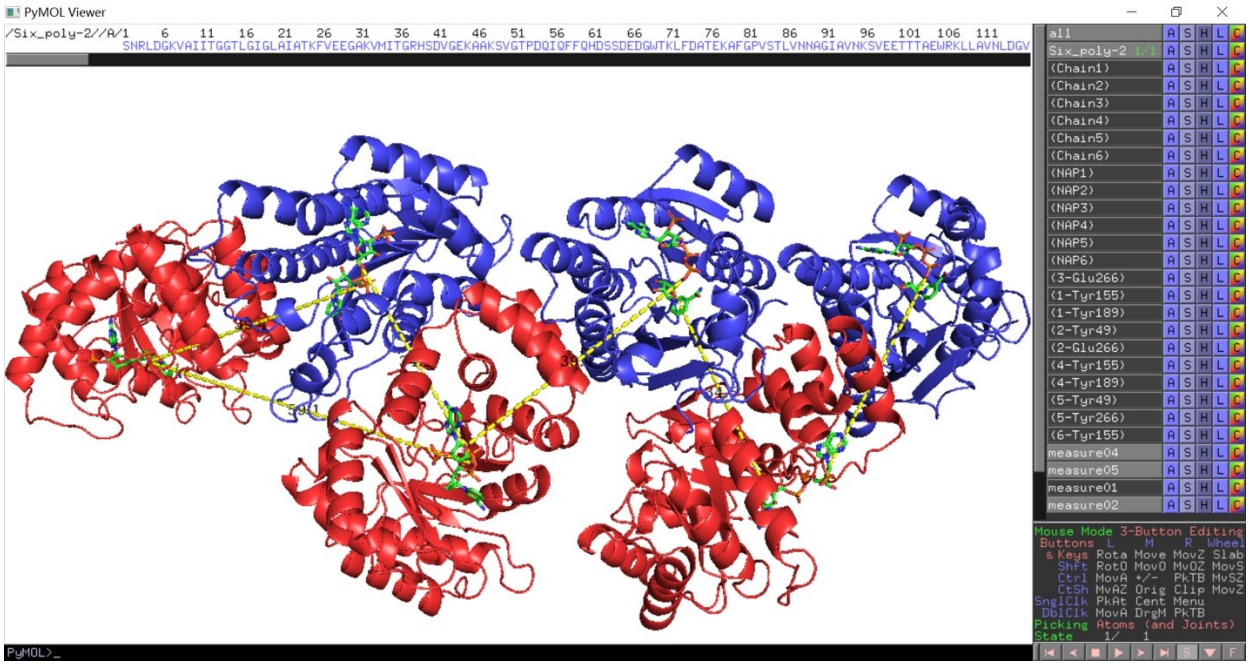

Figure S20. Intuitive interface of PyMOL for measuring the distance of AKR and ADH active sites

3. Abbreviation index

Table S7. Abbreviation index

Unabbreviated form	Abbreviation
Non-canonical amino acids	ncAAs
p-azido-L-phenylalanine	p-AzF
p-propargyloxy-L-phenylalanine	p-PaF
Aldo-keto reductase	AKR
Alcohol dehydrogenase	ADH
Orderly combi-crosslinked enzymes	O-CLEs
Site-specific combi-crosslinked enzymes	S-CLEs
Dibenzocycloocta-4a,6a-diene-5,11-diyne	DBA
Random combi-crosslinked enzyme aggregates	CLEAs
Confocal Laser Scanning Microscopy	CLSM
Nicotinamide adenine dinucleotide phosphate	NADPH

4. References

1. F. J. Isaacs, P. A. Carr, H. H. Wang, M. J. Lajoie, B. Sterling, L. Kraal, A. C. Tolonen, T. A. Gianoulis, D. B. Goodman, N. B. Reppas, C. J. Emig, D. Bang, S. J. Hwang, M. C. Jewett, J. M. Jacobson and G. M. Church, *Science*, 2011, **333**, 348-353.
2. M. J. Lajoie, A. J. Rovner, D. B. Goodman, H. R. Aerni, A. D. Haimovich, G. Kuznetsov, J. A. Mercer, H. H. Wang, P. A. Carr, J. A. Mosberg, N. Rohland, P. G. Schultz, J. M. Jacobson, J. Rinehart, G. M. Church and F. J. Isaacs, *Science*, 2013, **342**, 357-360.
3. M. B. Elowitz and S. Leibler, *Nature*, 2000, **403**, 335-338.
4. H. M. Li, R. Wang, A. M. Wang, J. Zhang, Y. C. Yin, X. L. Pei and P. F. Zhang, *ACS Sustain. Chem. Eng.*, 2020, **8**, 6466-6478.
5. E. Di Luccio, R. A. Elling and D. K. Wilson, *Biochem J*, 2006, **400**, 105-114.
6. H. Jornvall, B. Persson, M. Krook, S. Atrian, R. Gonzalez-Duarte, J. Jeffery and D. Ghosh, *Biochemistry*, 1995, **34**, 6003-6013.
7. M. Klimacek and B. Nidetzky, *J Biol Chem*, 2010, **285**, 30644-30653.
8. S. P. W. Pratul K. Agarwal, and Sharon Hammes-Schiffer, *J. Am. Chem. Soc.*, 2000, **122**, 4803-4812.
9. D.-H. P. Laurie A. LeBrun, S. Ramaswamy, and Bryce V. Plapp, *Biochemistry*, 2004, **43**, 3014-3026.
10. S. van Pelt, S. Quignard, D. Kubac, Y. S. B. Dimitry, F. van Rantwijk and R. A. Sheldon, *Green Chem.*, 2008, **10**, 395-400.

11. L. Li, J. O. Fierer, T. A. Rapoport and M. Howarth, *Journal of Molecular Biology*, 2014, **426**, 309-317.
12. R. Wang, J. Zhang, Z. Luo, T. Xie, Q. Xiao, X. Pei and A. Wang, *International Journal of Biological Macromolecules*, 2022, **205**, 682-691.
13. L. Q. Cao, F. van Rantwijk and R. A. Sheldon, *Org. Lett.*, 2000, **2**, 1361-1364.
14. B. A. S. and R. B. R., *Biocatalysis*, WILEY-VCH Verlag GmbH & Co. KGaA, Weinheim, 2004.
15. B. M., *Chem. Rev.*, 1995, **95**, 661-666.
16. M. Boudart, *Journal of Molecular Catalysis*, 1985, **30**, 27-38.
17. Y. Takaoka, A. Ojida and I. Hamachi, *Angewandte Chemie-International Edition*, 2013, **52**, 4088-4106.
18. V. Roullier, S. Clarke, C. You, F. Pinaud, G. Gouzer, D. Schaible, V. Marchi-Artzner, J. Piehler and M. Dahan, *Nano Letters*, 2009, **9**, 1228-1234.
19. S. R. Adams, R. E. Campbell, L. A. Gross, B. R. Martin, G. K. Walkup, Y. Yao, J. Llopis and R. Y. Tsien, *Journal of the American Chemical Society*, 2002, **124**, 6063-6076.
20. T. A. Ngo, E. Nakata, M. Saimura and T. Morii, *Journal of the American Chemical Society*, 2016, **138**, 3012-3021.
21. Y. H. P. Zhang, *Biotechnology Advances*, 2011, **29**, 715-725.
22. J. L. Lin, L. Palomec and I. Wheeldon, *Acs Catalysis*, 2014, **4**, 505-511.
23. L. Zhou, M. Morel, S. Rudiuk and D. Baigl, *Small*, 2017, **13**, 507-513.
24. S. Naseer, O. Y. Jie, X. Chen, S. J. Pu, Y. T. Guo, X. Zhang, D. L. Li and C. L. Yang, *International Journal of Biological Macromolecules*, 2020, **154**, 1490-1495.
25. E. Ricca, B. Brucher and J. H. Schrittwieser, *Advanced Synthesis & Catalysis*, 2011, **353**, 2239-2262.
26. D. M. Liu, J. Chen and Y. P. Shi, *Trac-Trends in Analytical Chemistry*, 2018, **102**, 332-342.
27. Y. Q. Lin, W. H. Jin, L. X. Cai, X. Liu, Y. Qiu and G. Y. Zhang, *Journal of Cleaner Production*, 2021, **314**, 127994.
28. F. A. Vicente, I. Plazl, S. P. M. Ventura and P. Znidarsic-Plazl, *Green Chemistry*, 2020, **22**, 4391-4410.

Author Contributions

[#] The authors contributed equally to this work.